



Maximum power point tracking of large-scale photovoltaic array



Ruo-li Tang^{a,d}, Zhou Wu^{b,c,*}, Yan-jun Fang^d

^a School of Energy and Power Engineering, Wuhan University of Technology, Wuhan, Hubei, China

^b The Key Laboratory of Dependable Service Computing in Cyber Physical Society of Ministry of Education, Chongqing University, Chongqing, China

^c School of Automation, Chongqing University, Chongqing, China

^d Department of Automation, Wuhan University, Wuhan, Hubei, China

ARTICLE INFO

Article history:

Received 31 December 2015

Received in revised form 27 March 2016

Accepted 17 May 2016

Keywords:

Large-scale photovoltaic array
Maximum power point tracking
Large-scale global optimization
Cooperative co-evolution

ABSTRACT

In partial shading conditions, reverse voltage may impose on the shaded photovoltaic modules and cause the “hot spot” problem. In this paper, a novel topological structure of photovoltaic array is proposed for operational safety and efficiency in possible partial shading, and the maximum power point tracking (MPPT) is also implemented on each photovoltaic module. This new structure consists of the photovoltaic module control device (PMCD) and branch voltage stabilization device (BVSD), which differentiate the MPPT at levels of each photovoltaic module (PVM-level MPPT) and minimum control unit (MCU-level MPPT). The MPPT of large-scale photovoltaic system can be formulated as a large-scale global optimization (LSGO) problem. Therefore, a novel multi-context cooperatively coevolving PSO (CCPSO-m) algorithm is proposed for solving the LSGO. Numerical result shows that the CCPSO-m outperforms some state-of-the-art algorithms evidently, and each photovoltaic module works on its own maximum power point effectively in the proposed structure of PV array. Finally, the large-scale photovoltaic system can achieve PVM-level (or MCU-level) MPPT, conquer the “hot spot” problem, and improve output power under complex environmental conditions significantly.

© 2016 Elsevier Ltd. All rights reserved.

1. Introduction

The increasing interest in greenhouse effect and other environmental issues, has asked for the development and installation of renewable energy systems, which could generate clean power with less cost and pollute emission. Some sustainable sources, e.g., wind, tidal, geothermal and solar energy, have become extremely important for replacing the fuel generation and improving the performance of energy supply, and some advanced control methods are also adopted in the process of power generation and utilization as well (Yin C. et al., 2014; Yin C. et al., 2015; Lai J.G. et al., 2016). For exploring the solar energy, the photovoltaic modules which are composed of several cells in series and parallel connections, are widely used in aerospace (Girish et al., 2007; Lee et al., 2015), architecture (Kibria et al., 2016; Wu and Xia, 2015), electric power generation (Choi and Lai, 2010; Kaabeche and Ibtouen, 2014), and other applications (Atmaca, 2015; Vinnichenko et al., 2014). However, due to varying environmental conditions, e.g., irradiance and temperature, photovoltaic module is usually regarded as an unstable

power supplier (Pierro et al., 2015). It is necessary to develop control methods of these photovoltaic modules in an attempt to ensure the security and efficiency of photovoltaic system.

In a solar generation system, the energy harvesting component is the photovoltaic array, which is usually composed of several modules in series and parallel connections. Under uniform irradiance condition, current and voltage of each photovoltaic module are almost the same, and the whole system works in good performance. However, when the irradiance becomes non-uniform, shading of even a single module can reduce the efficiency of the entire system significantly, and possibly cause permanent thermal damage (Maki and Valkealahti, 2013; Sullivan et al., 2013; Dein et al., 2013). Partial shading (or “non-uniform irradiance”) would also cause the so-called “hot spot” problem (Moreton et al., 2015). Shading modules in series branches may be imposed on reverse voltages and served as loads of photovoltaic system. As a result, these modules absorb power, and their surface temperature increases rapidly, which will cause permanent thermal damage of these shading branches. The gap of terminal voltages between different branches may also cause damage of the entire system. To conquer this “hot spot” weakness, the conventional method is to add bypass diodes across each module in parallel connections reversely, and to add blocking diodes in series connections at each branch (Ziar et al., 2014; d’Alessandro et al., 2014; Pennisi et al.,

* Corresponding author at: School of Automation, Chongqing University, Chongqing, China.

E-mail addresses: ruolitang@hotmail.com (R.-l. Tang), wuzhsky@gmail.com (Z. Wu), yjfang@whu.edu.cn (Y.-j. Fang).

2011). This method can ensure operational safety of the photovoltaic system, however, it also presents a significant reduction of the power output.

Suffering from the varying irradiance and temperature, effective control of current or voltage is necessary to introduce the maximum power output, which is defined as the maximum power point tracking (MPPT) problem. The conventional MPPT algorithms can be classified in two categories: online algorithms and offline algorithms. Online MPPT algorithms include the perturbation and observation method (P&O) (Piegari and Rizzo, 2010), the incremental conductance method (INC) (Tey and Mekhilef, 2014), and other P&O or INC variants (Petroni et al., 2011; Zan et al., 2013; Radjai et al., 2014). Offline MPPT algorithms are usually based on the mathematical model or empirical data of photovoltaic module, e.g., artificial neural networks (ANN) based MPPT algorithm (Kulaksiz and Akkaya, 2012), support vector machine (SVM) based MPPT algorithm (Chen et al., 2013), particle swarm optimization (PSO) based MPPT algorithm (Renaudineau et al., 2015), genetic algorithm (GA) based MPPT algorithm (Nafeh, 2011). In the existing online MPPT algorithms, e.g., the P&O, a perturbation is given to trigger the system, and then the feedback information is obtained for the MPPT control. Obviously, the repeated perturbation may cause system instability. In contrast, in the existing offline MPPT algorithms, no perturbation is required. The control input is computed beforehand, and the MPPT is usually implemented on each photovoltaic branch but not each module, so the resulted point cannot be the ideal maximum. Furthermore, when the photovoltaic array is really large (e.g., with thousands of modules), most algorithms show their inability to achieve the MPPT of each photovoltaic module (PVM-level MPPT). They fail to find the acceptable solution close to the global optimum.

In this study, a novel topological structure of photovoltaic array is proposed in an attempt to conquer the “hot spot” problem and achieve PVM-level MPPT. On one hand, a bidirectional Cuk converter as the “photovoltaic module control device (PMCD)” is utilized to control every two photovoltaic modules in a series branch. On the other hand, a boost converter as the “branch voltage stabilization device (BVSD)” is utilized to control terminal voltage of each parallel branch. In the new topological structure, each module in series is not required to work in the same current and each branch in parallel is not required to work in the same voltage either. Under the condition of uniform irradiance or partial shading, the PVM-level MPPT is applicable based on the proposed structure. Furthermore, the large-scale photovoltaic array with thousands of modules is studied to control each module's operating point, which is a large-scale global optimization problem. To solve this LSGO problem, a novel multi-context cooperatively coevolving particle swarm optimization (CCPSO-m) algorithm is also proposed in this paper. Numerical result shows that the CCPSO-m outperforms some state-of-the-art PSO variants on most of the test functions, and can solve the large-scale MPPT problem effectively.

The main contributions of this paper include three folds. Firstly, a novel topological structure of photovoltaic array based on PMCD and BVSD is proposed to conquer the “hot spot” problem. Secondly, a new MPPT method of large-scale photovoltaic array is studied in the approach of large-scale global optimization, in which the PVM-level (or MCU-level) MPPT is formulated into a LSGO problem. Thirdly, a new CCPSO-m algorithm is proposed in an attempt to improve the performance of some existing PSO variants on solving LSGO problems.

The rest of this paper is organized as follows: Section 2 presents an overview of some related works, including the conventional topological structure of photovoltaic array and some existing MPPT algorithms. Section 3 studies the structure and operational principle of PMCD and BVSD, and proposes a new

topological structure of large-scale photovoltaic array. In Section 4, the large-scale MPPT optimization problem is studied in terms of the related variables and fitness function. Section 5 studies the CCPSO-m algorithm, and gives some numerical results and analysis. Section 6 simulates the new structure of large-scale photovoltaic array and CCPSO-m based MPPT algorithm. Finally, this paper is concluded in Section 7.

2. Related work

2.1. Topological structure of photovoltaic array

It is well known that the output power of a single photovoltaic cell is relative small (only several Wp per cell). Therefore, a photovoltaic module is usually composed of several cells in series and parallel connections, and a photovoltaic array is also composed of many modules in series and parallel structures as well. The electrical characteristics of a photovoltaic cell can be analyzed via a well-established model (Laudani et al., 2014), which can be approximated by an equivalent circuit as shown in Fig. 1.

Shown as Fig. 1, I_{SC} denotes the current generated through a photovoltaic effect; I_D denotes the flowing-through current of the PN junction across the cell; R_s and R_p denote the series and parallel resistance of the model respectively; I_{sh} denotes the leakage current; V and I are the output voltage and current of the cell.

As photovoltaic array is composed of many modules in series and parallel connections, shading of even a single module can reduce the output power of the entire system significantly. Shading, especially partial shading is extremely harmful for photovoltaic system. Shown as Fig. 1, if the photovoltaic cell is totally shaded, the current source I_{SC} will be zero and the diode will become reversely biased. As connected in series with other cells under full irradiance condition, the current I flowing through the module will then travel through R_p . This leads to a voltage drop across R_s and R_p . Thus instead of generating power, this shaded cell will actually consume power and get hot, which will cause the “hot spot” problem. Furthermore, in terms of the branches in parallel, terminal voltage of the shaded branch will decrease immediately. Then, if the terminal voltage of full irradiance branch is larger than open circuit voltage of the shaded branch, the gap of terminal voltage between these branches may also cause a reverse current flowing through the shaded branch, which will cause the thermal damage to photovoltaic modules.

A widely used method to conquer the aforementioned problems is to utilize bypass diode and blocking diode. In this fold, a typical structure is given in Fig. 2. On one hand, a bypass diode is added in parallel with each photovoltaic module reversely. When a module is shaded to a certain degree, voltage drop of the shaded module will be larger than 0.7 V and the bypass diode will be turned on. In this way, the shaded module is protected by the bypass diode.

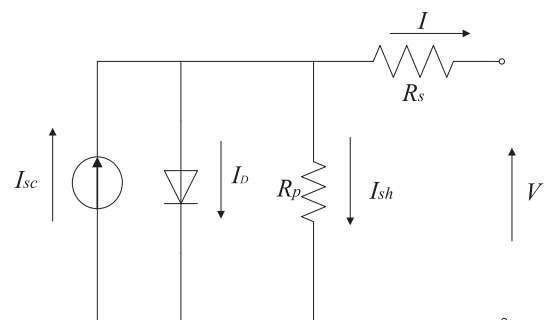


Fig. 1. Photovoltaic cell equivalent circuit.

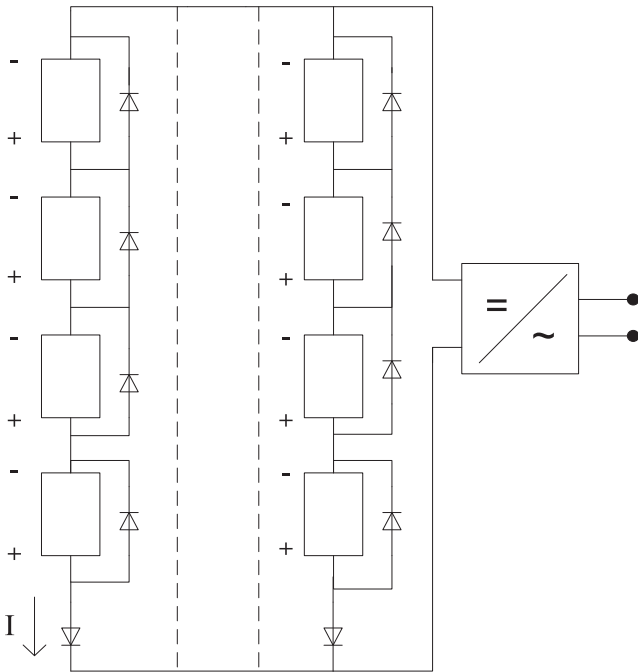


Fig. 2. Topological structure based on bypass-blocking diode.

On the other hand, the blocking diode is added in series at each branch, so that the reverse current is avoided if a branch is shaded.

2.2. MPPT algorithms of photovoltaic array

As an unstable power supplier, the photovoltaic cell is influenced by irradiance and temperature easily. Under certain environmental conditions, output power of a photovoltaic module is decided by its operating point, and the output power can be maximized by controlling the operating point of each module, which is the so-called MPPT. The process of MPPT must be dynamic, i.e. the operating point has to be continuously adjusted in response to the varying irradiance and temperature. As the environmental conditions are constantly changing, and meanwhile P - V curve itself exhibits non-linear characteristics, tracking the MPP is a complicated process especially when the photovoltaic array is composed of thousands of modules.

The existing MPPT algorithms can be classified in two major categories: online MPPT and offline MPPT. One popular online MPPT algorithm is the P&O method (Piegari and Rizzo, 2010; Koutroulis et al., 2001), in which a perturbation is given to trigger the system repeatedly, and then the feedback information is obtained for the MPPT control. Besides, the incremental conductance (INC) is another widely used online MPPT method due to its simplicity and reliability (Tey and Mekhilef, 2014; Radjai et al., 2014). INC adjusts the operating point U to move toward the MPP U_{\max} according to its conductance dI/dU , which is shown as Eq. (1).

$$\begin{cases} \text{if } dI/dU > -I/U \text{ then } U < U_{\max} \\ \text{if } dI/dU < -I/U \text{ then } U > U_{\max} \\ \text{if } dI/dU = -I/U \text{ then } U = U_{\max} \end{cases} \quad (1)$$

However, the basic P&O and INC methods inherently have several drawbacks (Jubaer and Zainal, 2015). Firstly, it causes an unending oscillation of the output power when tracking reaches the vicinity of maximum power point (MPP), which will reduce the energy harvesting efficiency. Secondly, P&O and INC are prone to lose tracking accuracy, especially under partial shading

conditions. Thirdly, when conditions of irradiance and temperature changes, it will cost a relatively long time to find the new MPP by perturbing the system continually.

To conquer these drawbacks, Jubaer and Zainal proposed an improved P&O by introducing a dynamic perturbation step-size to reduce oscillation, and they also introduced boundary conditions to prevent P&O diverging away from the MPP (Jubaer and Zainal, 2015). Femia et al. proposed a novel predictive & adaptive P&O method (Femia et al., 2005). Abdelsalam et al. proposed another P&O method with high performance for photovoltaic-based microgrids (Abdelsalam et al., 2011).

Offline MPPT method mainly contains the utilization of neural network (Kulaksiz and Akkaya, 2012), optimization algorithms (Benyoucef et al., 2015; Shi and Zhang, 2014) and some other advanced control algorithms. These methods are mainly based on the mathematical model or learning model of photovoltaic system. Generally, these methods can solve the complex and nonlinear problems easily. Xu et al. utilized the self-adaption BP-ANN for MPPT of photovoltaic system (Xu et al., 2012). In their study, the irradiance and temperature are regarded as the input variables of ANN, while the corresponding MPPs are regarded as the output values. The ANN is trained by a series of input and output data at first, and then it can give the MPPs of any certain environmental conditions. Liu et al. utilized the PSO algorithm for MPPT of distributed photovoltaic system (Liu et al., 2010). In their study, the current of each branch is regarded as the optimizing variable, and output power of the system is regarded as the fitness value. As a result, the MPPT problem is transformed into an optimizing problem, which can be solved by PSO.

However, most of the existing MPPT algorithms aim at tracking the MPP of a certain photovoltaic module or several modules in series or parallel connections. In terms of a large-scale photovoltaic array with thousands of modules, to track the MPP of each module in time become challenging, especially under complex and varying environmental conditions. In this study, a topological structure of large-scale photovoltaic array is developed, the large-scale MPPT is transformed into a LSGO problem, and a novel optimization method is then proposed to solve this problem.

3. A new topological structure for large-scale photovoltaic array

It is well known that the photovoltaic module is an unstable power supplier. Its I - V curve and P - V curve change frequently according to the variance of irradiance and temperature. The casual I - V curve and P - V curve under different environmental conditions can be plotted as Figs. 3 and 4 respectively. It can be found that the MPP of a photovoltaic module varies along with the irradiation and temperature. In order to maximize output power of the photovoltaic array under varying environmental conditions, it is necessary to track the MPP of each module in time.

3.1. Structure of PVM-level MPPT

To control the operating point of each photovoltaic module, two DC-DC converters are introduced to modify the conventional topological structure of photovoltaic array with thousands of modules in series and parallel connections. Although Lei has utilized a bidirectional converter to control two photovoltaic modules in series (Lei, 2011), there is few study on the structure and control method of a photovoltaic array with a lot of modules in series and parallel structures. In this study, a bidirectional Cuk converter is utilized as the photovoltaic module control device (PMCD), and a boost converter is also utilized as the branch voltage stabilization device (BVSD) in a new topological structure.

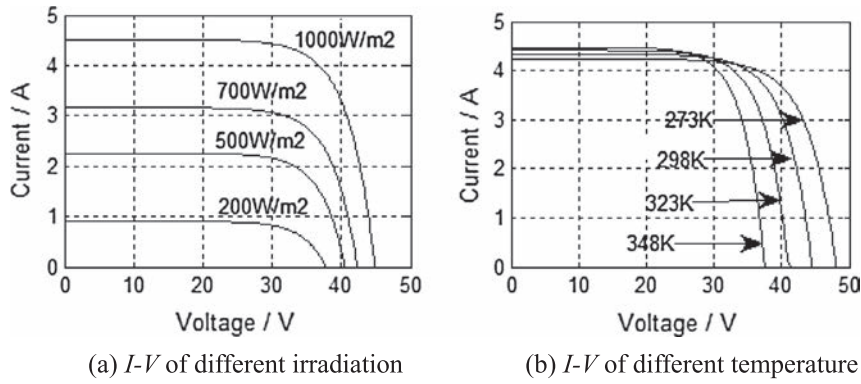


Fig. 3. *I-V* curve of a photovoltaic module under different environmental conditions.

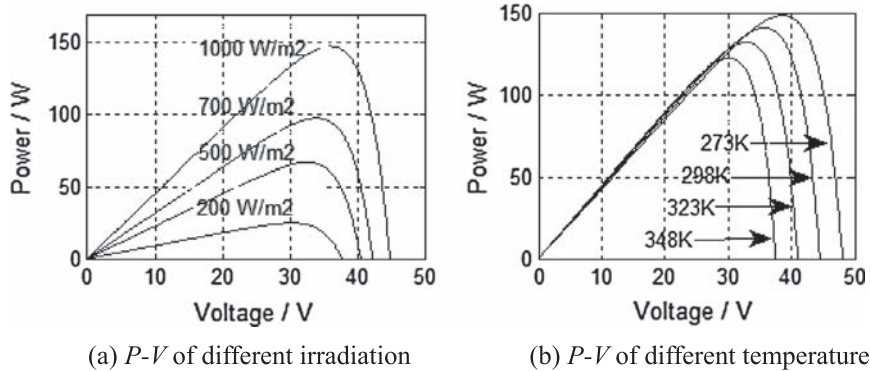


Fig. 4. *P-V* curve of a photovoltaic module under different environmental conditions.

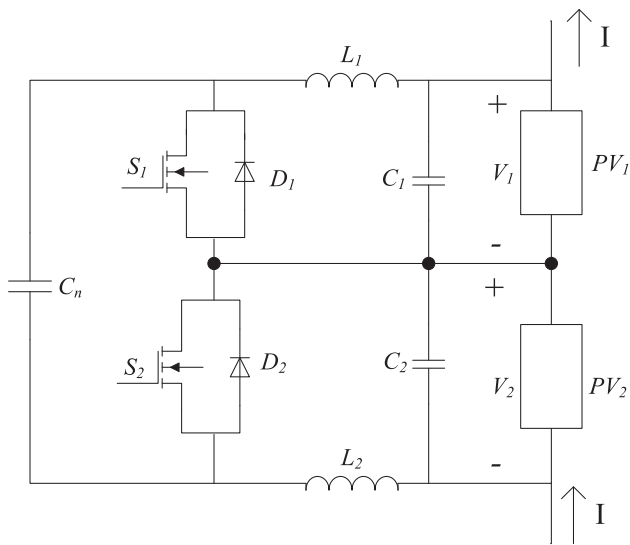


Fig. 5. Structure of bidirectional Cuk converter based PMCD.

Structure of a bidirectional Cuk converter and its connection with photovoltaic module are shown as Fig. 5. Under uniform irradiation, the two switches S_1 and S_2 keep open (off) and the converter does not work. Under partial shading conditions, e.g., PV_2 is shaded but PV_1 is not, S_1 - D_2 can be activated by a PWM wave imposed on S_1 . As a result, the converter is equivalent to a unidirectional Cuk circuit (V_1 is the input and V_2 the output), in which power is transferred from the V_1 terminal to the V_2 terminal. The duty cycle of S_1 can be controlled by a common proportional-integral (PI) controller, which is formulized as

$$K_1(s) = k_p[(V_{2ref} - V_2) - (V_{1ref} - V_1)] + \frac{k_i}{s[(V_{2ref} - V_2) - (V_{1ref} - V_1)]} \quad (2)$$

$$K_2(s) = 1 - K_1(s) \quad (3)$$

where K_1 and K_2 denote the duty cycle of S_1 and S_2 , k_p and k_i denote the parameters of the PI controller. V_1 and V_2 are the voltage of PV_1 and PV_2 respectively. V_{1ref} and V_{2ref} denote the reference values of V_1 and V_2 (control target), which are always set to the MPPs given by a certain MPPT algorithm.

Similarly, when PV_1 is shaded but PV_2 not, S_2 - D_1 will be active and the converter is equivalent to another unidirectional Cuk circuit (V_2 is the input and V_1 the output). Therefore, the operating point of both PV_1 and PV_2 can be controlled independently under varying environmental conditions.

Structure of a boost converter based BVSD and its connection with a photovoltaic branch is shown as Fig. 6. Each branch is connected in parallel through the BVSD, in which the terminal of each branch is the input of BVSD, and outputs of all the BVSDs are connected in parallel.

In a large-scale photovoltaic array with thousands of modules, all the modules are divided into several parts at first, and the structure of each part is the conventional series and parallel connection. In every series branch of each part, a PMCD is connected to every two PVs as Fig. 5, and the terminal of each branch is connected to a BVSD as Fig. 6. In this way, if the theoretical MPP of each PV is given to the corresponding device under certain environmental conditions, the PVM-level MPPT is applicable. The new structure of large-scale photovoltaic array is shown as Fig. 7.

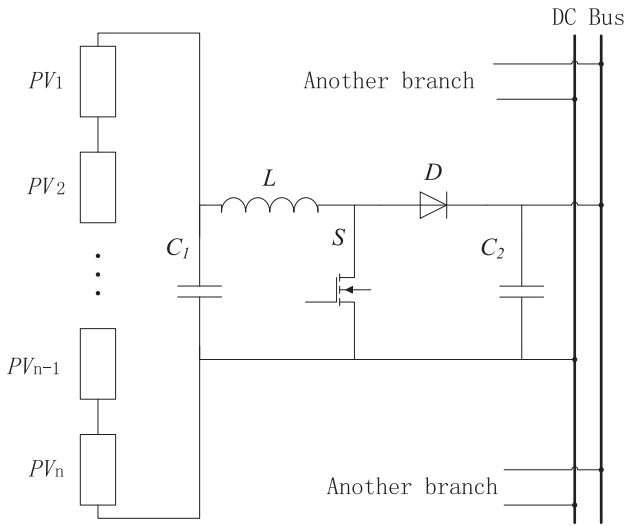


Fig. 6. Structure of boost converter based BVSD.

3.2. Structure of MCU-level MPPT

Regarding the increasing cost of the PVM-level structure, in which the PMCD and BVSD are connected to each photovoltaic module and branch, a minimum control unit (MCU) based topology structure can be introduced into the large-scale photovoltaic system. Each MCU consists of several photovoltaic modules connected in a certain topology. For example, 2 modules in parallel and 5 modules in series, which is shown as Fig. 8. In this MCU-level structure, a large-scale photovoltaic array with n_{pv-MCU} modules can be divided into n_{pv-MCU}/s_{MCU} MCUs, in which each one has s_{MCU} modules. As shown in Fig. 8, the MPPT control is imposed on each

MCU instead of each photovoltaic module, in an attempt to save cost of investment in practical applications.

4. The large-scale MPPT optimization problem

Many optimization algorithms are utilized to solve the MPPT problem, e.g., particle swarm optimization (PSO) (Shi and Zhang, 2014), genetic algorithm (GA) (Shaiek et al., 2013), artificial bee colony algorithm (ABC) (Benyoucef et al., 2015). However, complexity of the problem increases exponentially as dimensions increase, and most of the algorithms fail to find MPP of each module as the scale of photovoltaic array becomes extremely large. In order to achieve MPPT of large-scale photovoltaic array, the operating voltage of each module can be regarded as optimizing variable, and the output power of entire array can be regarded as the fitness value. Then the MPPT of large-scale photovoltaic array is transformed into a LSGO problem.

In the following simulation experiments, an engineering analytical model of silicon solar cells proposed in reference (Su et al., 2001) is utilized. The model matches $I-V$ curve of real photovoltaic cells well, which can be formulized as

$$\begin{cases} I = I_{SC} \left\{ 1 - C_1 \left[\exp \left(\frac{V}{C_2 V_{oc}} \right) - 1 \right] \right\} \\ C_1 = \left(1 - \frac{I_m}{I_{SC}} \right) \exp \left(- \frac{V_m}{C_2 V_{oc}} \right) \\ C_2 = \left(\frac{V_m}{V_{oc}} - 1 \right) \left[\ln \left(1 - \frac{I_m}{I_{SC}} \right) \right]^{-1} \end{cases} \quad (4)$$

$$\begin{cases} I_{SC} = I_{SCref} \frac{S}{S_{ref}} (1 + a\Delta T) \\ V_{oc} = V_{ocref} \ln(e + b\Delta S)(1 - c\Delta T) \\ I_m = I_{mref} \frac{S}{S_{ref}} (1 + a\Delta T) \\ V_m = V_{mref} \ln(e + b\Delta S)(1 - c\Delta T) \end{cases} \quad (5)$$

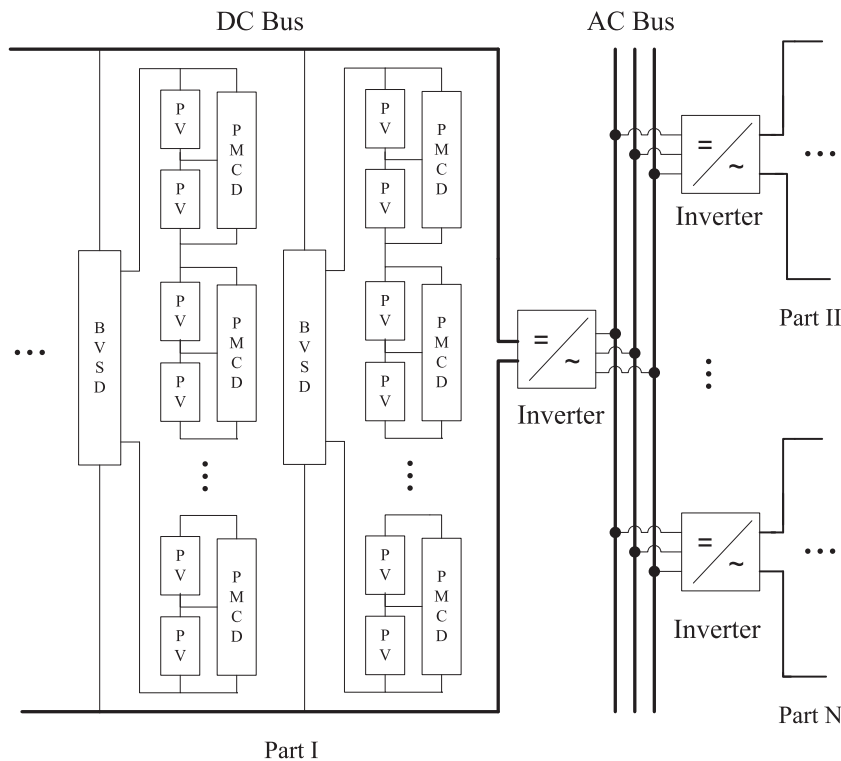


Fig. 7. Topological structure of large-scale photovoltaic array based on PMCD and BVSD.

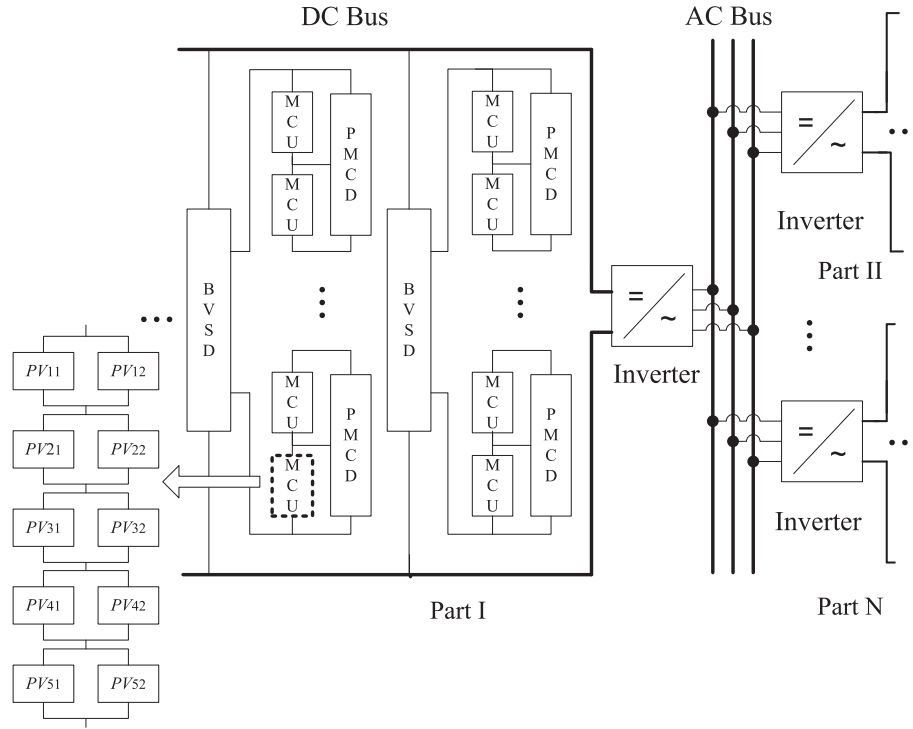


Fig. 8. Topological structure of large-scale photovoltaic array based on MCU.

where $S_{ref} = 1000 \text{ W/m}^2$ is the reference irradiation, and $T_{ref} = 25 \text{ }^\circ\text{C}$ is the reference temperature. $\Delta S = S - S_{ref}$ is the difference between irradiation S and its reference S_{ref} , and $\Delta T = T - T_{ref}$ is the difference between temperature T and its reference T_{ref} . I_{SCref} , V_{OCref} , I_{mref} and V_{mref} are four main parameters of the photovoltaic module, which can be provided by the producer. As suggested in reference [Su et al. \(2001\)](#), a , b and c are compensation factors of the model, which equal to $0.0025/(\text{ }^\circ\text{C})$, $0.0005/(\text{W/m}^2)$ and $0.00288/(\text{ }^\circ\text{C})$, respectively. e denotes the natural logarithm which equals to 2.71828.

4.1. Model of PVM-level MPPT

In order to achieve the PVM-level MPPT, operating voltage of each module is regarded as the optimizing variable, and the reciprocal of the total output power is regarded as the objective function value. As a result, the large-scale MPPT problem in PVM-level can be formulized as

$$\min \frac{1}{\sum_{i=1}^{n_{pv}} V_i I_{SCi} \left\{ 1 - C_{1i} \left[\exp \left(\frac{V_i}{C_{2i} V_{OCi}} \right) - 1 \right] \right\}} \quad (6)$$

s.t. $V_i \in [V_l, V_u]$

where n_{pv} denotes the number of photovoltaic modules in the large-scale array. V_i denotes the operating voltage of the i th module. V_l and V_u denote the lower and upper bound of V_i respectively. In general, V_l is set to 0 and V_u is usually set to the largest open circuit voltage (V_{OC}) of the module under extreme conditions.

4.2. Model of MCU-level MPPT

In terms of the MCU-level MPPT, P - V (or P - I) curve of the shaded MCUs become multimodal under partial shading conditions, which causes the increasing complexity of MPPT. To regard the current of each MCU as optimizing variable, and the output power of the entire system as fitness function value, the MCU-level MPPT can be formulized as

$$\min \frac{1}{\sum_{i=1}^{n_{MCU}} \sum_{j=1}^{n_{SC}} I_i C_{2ij} V_{OCij} \log \left[\frac{1}{C_{1ij}} \left(1 - \frac{I_i}{n_{pc} I_{SCij}} \right) + 1 \right]} \quad (7)$$

s.t. $I_i \in [I_l, I_u]$

where n_{MCU} denotes the number of MCUs, which equals to n_{pv-MCU} / S_{MCU} . n_{pv-MCU} represents the number of photovoltaic modules in the large-scale array, and S_{MCU} represents the number of photovoltaic modules in each MCU. I_i ($i = 1, 2, \dots, n_{MCU}$) is current of the i th MCU, I_l and I_u are the lower and upper bound of I_i . In general, I_l is set to 0, and I_u is usually set to the short-circuit current of each MCU under extreme conditions. C_{1ij} , C_{2ij} , V_{OCij} and I_{SCij} denote the corresponding parameters: C_1 , C_2 , V_{OC} and I_{SC} of the photovoltaic module PV_{jt} ($j = 1, 2, \dots, n_{SC}$; $t = 1, 2, \dots, n_{pc}$) in the i th MCU. n_{sc} and n_{pc} denote the modules in series and in parallel connections within each MCU. Obviously, in the structure shown as [Fig. 8](#), n_{sc} and n_{pc} equal to 5 and 2 respectively.

5. Multi-context cooperatively coevolving PSO

In order to solve the MPPT problem of a large-scale photovoltaic system with thousands of modules, an effective large-scale optimization algorithm is required. Large-scale global optimization (LSGO) problem, which appears frequently in modern engineering applications, attracts attention of many researchers. The search space and interactions between variables may grow exponentially as the dimension increases, so to optimize LSGO problem becomes extremely difficult. To conquer these difficulties, a cooperative coevolution (CC) framework based on a philosophy of “divide and conquer” is proposed by Potter and Jong ([Potter and Jong, 1994](#)). Based on the basic CC framework, Van den Bergh and Engelbrecht proposed two improved algorithms CPSO-S_K and CPSO-H_K ([Van den Bergh and Engelbrecht, 2004](#)). However, these two algorithms only tested on functions of up to 30 dimensions, and that is far away from LSGO. Li and Yao applied random grouping and adaptive weighting mechanism and proposed the CCPSO ([Li and Yao, 2009](#)) and CCPSO2 ([Li and Yao, 2012](#)) algorithms. In this study, a

novel CCPSO-m algorithm is proposed in an attempt to improve the performance on LSGO, and then the CCPSO-m is utilized to solve the PVM-level and MCU-level MPPT problem of large-scale photovoltaic array.

5.1. Multi-context CC framework

In the basic CC framework, a high-dimensional problem is decomposed into several relatively low-dimensional subcomponents, and each of these subcomponents is evolved by a separate subpopulation. Each individual in each subcomponent represents only several dimensions of the search space and it is impossible to compute its fitness value directly without a context. For this purpose, the best particle of each subcomponent is used to combine a single context vector (Potter and Jong, 1994), and based on this context vector, searching efforts will be made on a small portion of components for each subcomponent while the other components keep fixed and same as the context vector.

It has been proved that the basic CC framework can solve some problems with a relatively high dimension, however, it also fails to find the global optimum as complexity or dimension becomes large enough (Van den Bergh and Engelbrecht, 2004; Li and Yao, 2009; Li and Yao, 2012). In this study, p context vectors are introduced to modify the single-context mechanism of basic CC (it is obvious that when $p = 1$, the new framework equals to basic CC), in an attempt to increase the possibility of evolving each subcomponent towards the global optimum. These context vectors are initialized with the best p particles in the D -dimensional initialized population. When evolve a certain subcomponent, each particle can choose one context vector from the p ones randomly.

Furthermore, in order to evolve all the context vectors, a crossover mechanism of these context vectors is introduced in every c iterations (cycles), where c can be regarded as a parameter of the new algorithm. The process of crossover can be designed as follows: composing a new context vector (CV_{new}) by interchanging variables randomly between the best one (CV_{best}) and the worst one (CV_{worst}) of the p existing context vectors, updating CV_{worst} with CV_{new} if it is better. The process described above is repeated for k times, comparing and updating the newest CV_{worst} of each time with $CV_{new1}, CV_{new2}, \dots, CV_{newk}$ respectively. This crossover mechanism aims to evolve all the context vectors and explore some potential optimums with a relatively less cost.

5.2. CCPSO-m algorithm

In addition to the multi-context and its crossover mechanism, in the new CCPSO-m algorithm, a particle position updating rule based on Gaussian distribution is introduced, which is formulized as Eq. (8)

$$P_j \cdot x_i(t+1) = \frac{1}{2}(P_j \cdot y_i(t) + \hat{y}(t)) + N(0, 1)|P_j \cdot y_i(t) - \hat{y}(t)| \quad (8)$$

where $P_j \cdot y_i(t)$ denotes the personal best position of the i th particle in j th subcomponent, and $\hat{y}(t)$ denotes the global best position. $P_j \cdot x_i(t+1)$ denotes the next position of the i th particle in j th subcomponent, and $N(0, 1)$ denotes a standard Gaussian distribution. Furthermore, the random grouping and dynamic group size proposed in reference Yang et al. (2008) are also applied in CCPSO-m. The procedure of CCPSO-m can be illustrated in the following steps

- (1) A population of NP particles is initialized in the D -dimensional searching space, and initialized the global best position and p context vectors.
- (2) Decomposing the searching space into several subcomponents randomly at the beginning of each iteration.

- (3) Recording the fitness value of the global best before and after each iteration, if there is no improvement of this fitness value, a new group size s (number of variables in each subcomponent) is chosen uniformly at random from a set \mathbf{S} ; otherwise, the group size s remains unchanged. Here \mathbf{S} is a set of group size in advance, e.g., $\mathbf{S} = \{5, 10, 20, 50, 100, 200\}$. Obviously, each subcomponent has D/s dimensions.
- (4) For each subcomponent, choosing a context vector for each particle randomly and update position of each particle using Eq. (8).
- (5) Updating personal best position of each particle and its corresponding context vector.
- (6) In every c iterations (cycles), executing the crossover process of the p context vectors as described in Section 5.1.
- (7) If the stopping criteria are not satisfied, go to step (2).

5.3. CCPSO-m on benchmark functions

The performance of CCPSO-m is empirically evaluated on a comprehensive set of 6 benchmark functions (F_1 to F_6), which are proposed in the CEC' 2008 special section on LSGO. F_1 and F_2 are unimodal functions, and F_3 to F_6 are multimodal functions. F_1, F_4, F_6 are separable functions, and F_2, F_3, F_5 are non-separable functions. Details of these functions can be found in reference Li and Yao (2012).

Performances of some state-of-the-art PSO variants are compared with CCPSO-m, including CCPSO- S_K (Van den Bergh and Engelbrecht, 2004), CCPSO- S_K -rg-aw (Li and Yao, 2009) and CCPSO2 (Li and Yao, 2012), which are described as follows

- CCPSO- S_K : Identical to the CCPSO- S_K described in Van den Bergh and Engelbrecht (2004), where K is the number of subcomponents and is set to 10 in the following experiment.
- CCPSO- S_K -rg-aw: CCPSO- S_K employing both random grouping and adaptive weighting, which is proposed in Li and Yao (2009). K is also set to 10 in the following experiment.
- CCPSO2: Proposed in Li and Yao (2012) and the dynamic group size is set to $\mathbf{S} = \{2, 5, 10, 20, 50\}$.
- CCPSO-m: Dynamic group size is set to $\mathbf{S} = \{2, 5, 10, 20, 50\}$, number of context vectors (p) is set to 5, crossover is executed in every 50 cycles ($c = 50$), and repeat for 30 times ($k = 30$).

Experiments are conducted on the 6 test functions of 1000 dimensions. For each test function, the average results of 25 independent runs are recorded, and the maximum number of fitness evaluations (Max_FES) of each run is set to $5.0E+06$, i.e., $5 * 10^6$. c_1 and c_2 of each PSO variant are set to 1.49, and the common "linear decreasing weight" ω , which decreases from 0.9 to 0.4 linearly, are also utilized. Results of this experiment are shown as Table 1, the best, worst and average performance of 25 independent runs, as well as the standard deviation, are listed in the table.

Shown as Table 1, in which the best performer is in bold, CCPSO-m outperforms the other compared algorithms on F_1, F_3, F_4, F_5 and F_6 . In terms of F_2 , there is no statistical difference between CCPSO-m and CCPSO2, but they are slightly better than CCPSO- S_K and CCPSO- S_K -rg-aw. CCPSO-m can find the global optimum 0 with an enough accuracy when optimizing F_1 and F_4 , much better than the performance of CCPSO- S_K and CCPSO- S_K -rg-aw, and even better than CCPSO2, which only has an accuracy of $7.35E-07$ and $5.76E-03$ respectively. A conclusion can be drawn from Table 1 that the performance of CC framework has been improved with the introduction of multi-context and crossover mechanism, and the proposed CCPSO-m outperforms some state-of-the-art CC-based algorithms compared on LSGO with up to 1000 dimensions.

Table 1
Comparison of PSO variants on CEC' 08 (F_1 to F_6) LSGO of 1000 dimensions.

Functions		CCPSO- S_K	CCPSO- S_K -rg-aw	CCPSO2	CCPSO-m
F_1	Average	4.96E+03	1.65E+04	7.35E-07	0.00E+00
	Worst	5.76E+03	1.75E+04	1.98E-06	0.00E+00
	Best	4.16E+03	1.55E+04	3.09E-07	0.00E+00
	Std	3.98E+02	5.49E+02	4.47E-07	0.00E+00
F_2	Average	7.10E+01	5.58E+01	1.58E+01	1.42E+01
	Worst	7.40E+01	5.82E+01	1.69E+01	1.55E+01
	Best	6.65E+01	4.90E+01	1.50E+01	1.12E+01
	Std	1.90E+00	2.04E+00	4.52E-01	1.39E+00
F_3	Average	1.82E+07	3.59E+08	2.06E+03	4.61E+01
	Worst	3.42E+07	3.93E+08	2.35E+03	9.10E+01
	Best	1.10E+07	3.10E+08	1.77E+03	6.68E+00
	Std	4.78E+06	2.22E+07	1.51E+02	2.17E+01
F_4	Average	2.67E+03	1.12E+03	5.76E-03	0.00E+00
	Worst	2.89E+03	1.16E+03	9.92E-03	0.00E+00
	Best	2.55E+03	1.09E+03	3.30E-03	0.00E+00
	Std	7.73E+01	2.12E+01	1.82E-03	0.00E+00
F_5	Average	4.49E+01	1.50E+02	3.15E-03	4.72E-11
	Worst	5.52E+01	1.59E+02	1.48E-02	9.22E-11
	Best	3.93E+01	1.41E+02	3.08E-08	6.33E-12
	Std	3.66E+00	4.56E+00	4.95E-03	1.14E-11
F_6	Average	4.61E+00	6.49E+00	3.27E-05	6.83E-13
	Worst	4.84E+00	6.66E+00	4.18E-05	9.43E-13
	Best	4.42E+00	6.31E+00	2.25E-05	2.63E-13
	Std	9.98E-02	8.62E-02	6.10E-06	1.12E-13

6. Simulation analysis of the large-scale MPPT

In this section, the new topological structure is simulated on a small-scale photovoltaic array with 4 modules to verify its effectiveness. With the application of CCPSO-m, the PVM-level and MCU-level MPPT control is also simulated on a large-scale photovoltaic array.

6.1. Comparison of PMCD-BVSD based system and bypass-blocking-diode based system

In order to verify the effectiveness of PMCD-BVSD topological structure, a small-scale photovoltaic array with 4 modules is simulated under different environmental conditions, and the common bypass-blocking diode system is studied for comparison. Structures of the two systems are shown as Figs. 9 and 10. Parameters of each module are as follows: the maximum output power (P_m)

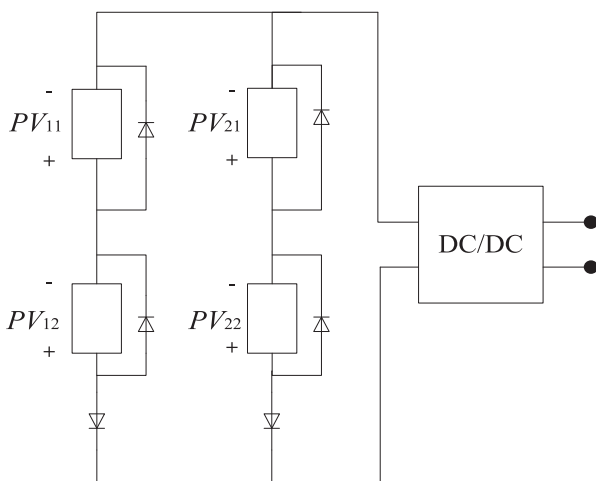


Fig. 9. Structure of bypass-blocking-diode system.

under the normal condition (1000 W/m^2 and 25°C) is 46.5 W , and its corresponding operating voltage (V_m) is 15.78 V ; under the shaded condition (500 W/m^2 and 25°C), P_m and V_m equal to 21.8 W and 14.78 V respectively.

The two systems are compared in the same environmental conditions. Irradiation of all the modules are 1000 W/m^2 from 0 s to 2 s , except that PV_{12} is shaded for a second ($S_{12} = 500 \text{ W/m}^2$ when $1 \text{ s} < t < 2 \text{ s}$). The temperature is set to 25°C during the entire process. The output power of PV_{12} (shaded module) and PV_{11} (full irradiation module in shaded branch), and output power of the system is shown as Figs. 11 and 12.

Shown as the figures, when PV_{12} is shaded with irradiation 500 W/m^2 , output power of PV_{12} in the bypass-blocking diode system decreases to 20.6 W from 46.5 W . In the PMCD-BVSD system, the output power keeps to 21.8 W , which is the theoretical MPP of the shaded environment. In the PMCD-BVSD system, after a short-time adjustment (0.3 s), output power of PV_{11} recovers back to 46.5 W , which is the theoretical MPP of normal irradiation. However, in the bypass-blocking diode system, output power of PV_{11} decreases to 29.3 W . The overall output power is 161.1 W in the PMCD-BVSD system but only 143.0 W in the bypass-blocking diode system.

Furthermore, when the system is under complex environmental conditions, which means irradiation of each module is different from each other, e.g., $S_{11} = 700 \text{ W/m}^2$, $S_{12} = 300 \text{ W/m}^2$, $S_{21} = 1000 \text{ W/m}^2$, $S_{22} = 500 \text{ W/m}^2$, simulation results are shown in Table 2, where *system-diode* denotes the bypass-blocking diode based system and *system-device* denotes the PMCD-BVSD based system.

In Table 2, under complex environmental conditions, the *system-device* proposed in this study outperforms the common *system-diode* evidently. In *system-device*, each module operates around its own theoretical MPP, however, certain deviations exist in *system-diode*. Output power of *system-diode* is 78.25 W and 104.01 W in the two experiments. In contrast, output power of *system-device* is 112.19 W and 116.59 W , which exceed the *system-diode* about 43.4% and 12.09% respectively. In a word, with the utilization of PMCD and BVSD, each photovoltaic module can stably operate around its given value. As a result, in terms of a large-scale photovoltaic array, an effective MPPT algorithm is required to find MPPs of all the modules, which are then given to each PMCD and BVSD as the reference values in time.

6.2. Comparison of different MPPT methods

6.2.1. PVM-level MPPT of large-scale photovoltaic system

In this section, the CCPSO-m algorithm is verified for the PVM-level MPPT of large-scale photovoltaic array. The number of modules n_{pv} is set to 2000 in this simulation. CCPSO-m is compared with the basic PSO and other state-of-the-art algorithms.

The basic PSO with constriction coefficient is utilized for comparison, in which c_1 and c_2 are set to 2.05, and $\chi = 0.729$ (Clerc and Kennedy, 2002; Eberhart and Shi, 2000). In addition, some state-of-the-art algorithms are also utilized for comparison, including two PSO variants: CCPSO- S_K and CCPSO2 described in Section 5.3, and a DE variant: SaDE (Qin and Suganthan, 2005). Parameter settings of CCPSO- S_K and CCPSO2 are the same as Section 5.3, and parameters of SaDE are the same as its original paper.

Settings of the photovoltaic module parameters described by Eqs. (4) and (5) are as follows: $I_{SCref} = 4.515 \text{ A}$, $V_{OCref} = 44.852 \text{ V}$, $I_{mref} = 3.989 \text{ A}$, and $V_{mref} = 36.895 \text{ V}$. For each compared method, the average results of 25 independent runs are recorded. Population size of all the algorithms is set to 15, and maximum number of fitness evaluations (Max_FES) is set to $5.0E+05$. In CCPSO-m and CCPSO2, the dynamic group size is set to $S = \{10, 20, 50, 100\}$, and the number of context vectors of CCPSO-m is set to 5. Consid-

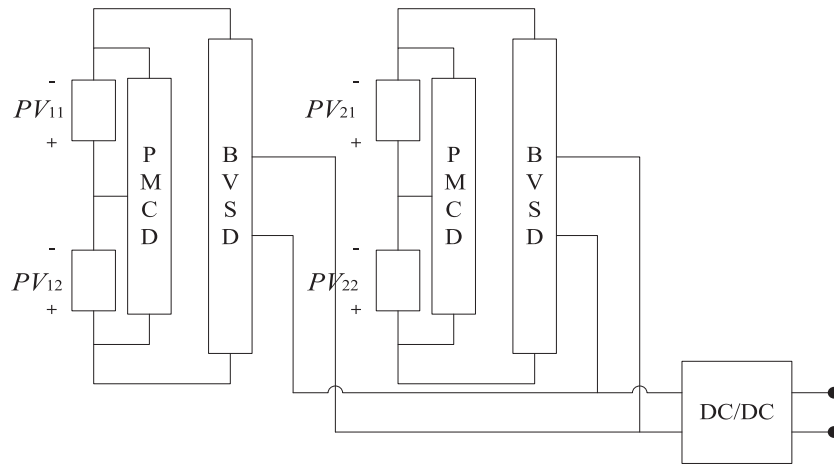


Fig. 10. Structure of PMCD-BVSD system.

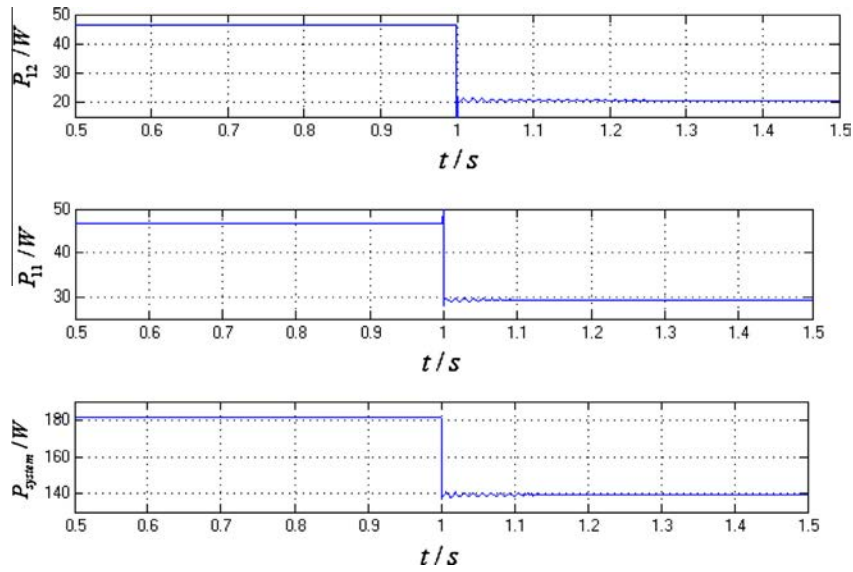


Fig. 11. Output power of bypass-blocking diode based system when PV_{12} is shaded.

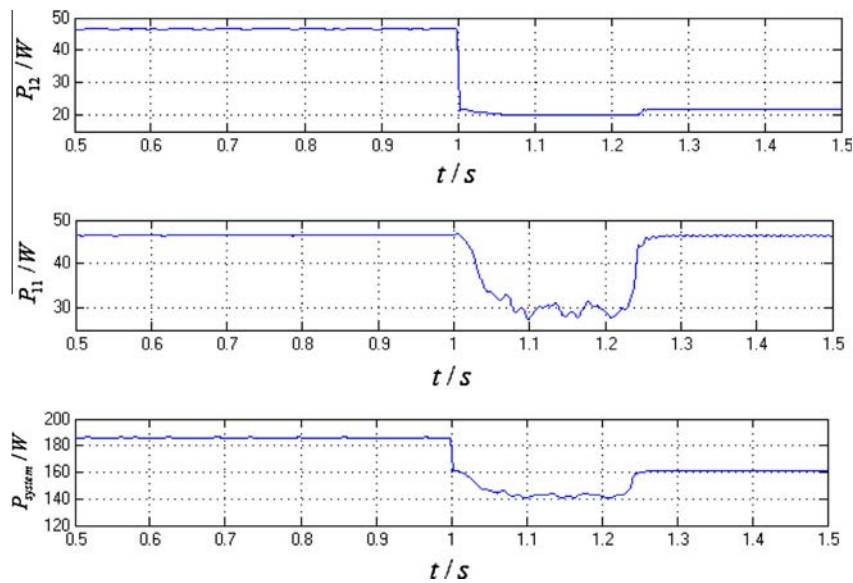


Fig. 12. Output power of PMCD-BVSD based system when PV_{12} is shaded.

Table 2
Comparison of the two systems under complex environmental conditions.

Irradiation (W/m^2)	Operating point of system-diode (V)	Operating point of system-device (V)	Theoretical MPP (V)	Output power of system-diode (W)	Output power of system-device (W)	Power promotion (%)
$S_{11} = 700$	$V_{11} = 18.19$	$V_{11} = 15.27$	$V_{r11} = 15.28$	78.25	112.19	43.4
$S_{12} = 300$	$V_{12} = 14.19$	$V_{12} = 14.05$	$V_{r12} = 14.04$			
$S_{21} = 1000$	$V_{21} = 18.46$	$V_{21} = 15.78$	$V_{r21} = 15.78$			
$S_{22} = 500$	$V_{22} = 13.92$	$V_{22} = 14.77$	$V_{r22} = 14.78$			
$S_{11} = 900$	$V_{11} = 17.32$	$V_{11} = 15.61$	$V_{r11} = 15.62$	104.01	116.59	12.09
$S_{12} = 700$	$V_{12} = 15.07$	$V_{12} = 15.28$	$V_{r12} = 15.28$			
$S_{21} = 600$	$V_{21} = 15.91$	$V_{21} = 15.05$	$V_{r21} = 15.04$			
$S_{22} = 400$	$V_{22} = 14.81$	$V_{22} = 14.44$	$V_{r22} = 14.45$			

ering the terrible environmental conditions, optimizing space of operating voltage V_i ($i = 1, 2, \dots, 2000$) is set to $[0, 60]$. The environmental conditions are as follows: PV_1 to PV_{500} are under $1000 W/m^2$ and $25^\circ C$ (with theoretical MPP $147.6749 W$), PV_{501} to PV_{1000} are under $600 W/m^2$ and $20^\circ C$ (with theoretical MPP $81.9742 W$), PV_{1001} to PV_{1500} are under $200 W/m^2$ and $16^\circ C$ (with theoretical MPP $24.9042 W$), PV_{1501} to PV_{2000} are under $100 W/m^2$ and $15^\circ C$ (with theoretical MPP $12.1322 W$). As a result, the theoretical MPP of the entire array is about $1.3334E+05 W$, which can be computed with the point by point comparison (PPC). In this comparison, results are shown as Table 3.

In Table 3, PSO and CCPSO- S_K fail to find the global optimum of a 2000-dimensional MPPT problem due to the “curse of dimension”, and the relative errors are 31.44% and 29.81% respectively. CCPSO2 and SaDE perform much better than PSO and CCPSO- S_K , however, they still have the relative errors of 2.15% and 3.49% respectively. CCPSO-m obtains the best performance, and can find the maximum power point with the highest accuracy.

6.2.2. MCU-level MPPT of large-scale photovoltaic system

CCPSO-m, CCPSO2, CCPSO- S_K , SaDE and PSO are utilized in MCU-based MPPT of the large-scale photovoltaic system. The number of MCUs n_{MCU} is set to 2000 in this simulation, each MCU contains 10 modules as connected as Fig. 8. Note that the entire photovoltaic array then contains 20,000 modules. Under the reference environmental condition of $1000 W/m^2$ and $25^\circ C$, the short-circuit current of each module is around 4.52 A. As a result, to consider the terrible environmental conditions with redundancy current, decision space of I_i ($i = 1, 2, \dots, 2000$) in Eq. (7) is set to $[0, 15]$ A. The complex environmental conditions are set as Table 4, and P - V curve of MCU under each environmental condition is shown in Fig. 13. Similarly, the theoretical MPP of the entire array is about $9.0976E+05 W$. The other parameter settings of each compared algorithm are the same as Section 6.2.1. The average results of 25 independent runs are shown as Table 5.

In a large-scale photovoltaic system based on the MCU-level structure, the MPPT can be solved by optimizing a large-scale multimodal problem. In Table 5, performance of the compared algorithms deteriorates when the MCUs are under complex environmental conditions. PSO and CCPSO- S_K have the worst performance with relative errors 44.69% and 41.51% respectively, which are far away from the global optimum. CCPSO2 and SaDE

Table 3
Comparison of different MPPT methods.

Method	Result (W)	Error (%)
CCPSO-m	1.3332757E+05	0.01
CCPSO2	1.3047035E+05	2.15
CCPSO- S_K	9.3589306E+04	29.81
SaDE	1.2869569E+05	3.49
PSO	9.1414916E+04	31.44

Table 4
Settings of the complex environmental conditions.

MCU index	Modules	Irradiation (W/m^2)	Temperature ($^\circ C$)	Theoretical MPP (W)
1–500	PV_{11}, PV_{12}	1000	25	5.7350072E+02
	PV_{21}, PV_{22}	800	22	
	PV_{31}, PV_{32}	600	20	
	PV_{41}, PV_{42}	400	18	
	PV_{51}, PV_{52}	200	16	
501–1000	PV_{11}, PV_{12}	200	16	3.7302576E+02
	PV_{21}, PV_{22}	100	15	
	PV_{31}, PV_{32}	800	22	
	PV_{41}, PV_{42}	600	20	
	PV_{51}, PV_{52}	400	18	
1001–1500	PV_{11}, PV_{12}	400	18	4.9351633E+02
	PV_{21}, PV_{22}	200	16	
	PV_{31}, PV_{32}	100	15	
	PV_{41}, PV_{42}	1000	25	
	PV_{51}, PV_{52}	800	22	
1501–2000	PV_{11}, PV_{12}	1000	25	3.7948283E+02
	PV_{21}, PV_{22}	600	20	
	PV_{31}, PV_{32}	400	18	
	PV_{41}, PV_{42}	200	16	
	PV_{51}, PV_{52}	100	15	

Table 5
Comparison of different methods on MPPT of MCU based system.

Method	Result (W)	Error (%)
CCPSO-m	9.0855074E+05	0.13
CCPSO2	8.5317634E+05	6.22
CCPSO- S_K	5.3208647E+05	41.51
SaDE	6.6536143E+05	26.86
PSO	5.0323447E+05	44.69

obtain relative errors 6.22% and 26.86% respectively, which are much better than PSO and CCPSO- S_K . However, they cannot outperform CCPSO-m, which achieve the best performance with the relative error 0.13%.

7. Conclusion

A new MPPT method of large-scale photovoltaic system is proposed to conquer the “hot spot” problem, to ensure operational safety and to improve the output power under complex environmental conditions. This study mainly includes two aspects: topological structure and MPPT algorithm. Firstly, a bidirectional Cuk converter is utilized to control the operating point of each module, and a boost converter is utilized to control the terminal voltage of each branch. Therefore, a new topological structure is proposed based on these two devices. Secondly, MPPT of large-scale photovoltaic system is modeled as the LSGO, and a novel multi-context

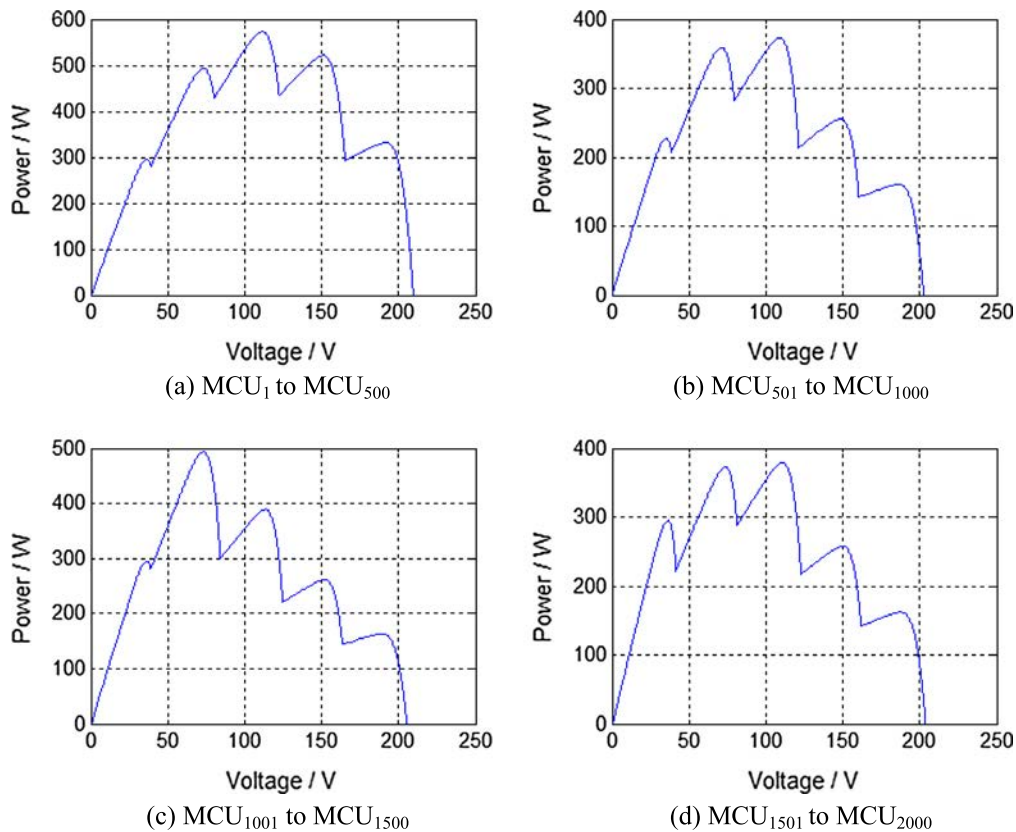


Fig. 13. P - V curve of MCU under partial shading condition.

cooperatively coevolving PSO algorithm (CCPSO-m) is proposed to solve this large-scale problem.

According to the simulation results, each photovoltaic module can operate around its reference value stably on the new structure. The proposed CCPSO-m has competitive performance with other state-of-the-art algorithms. CCPSO-m is successfully applied to the MPPT problem of a large-scale photovoltaic system with 2000 modules, and even 20,000 modules in the MCU-based structure. According to the numerical results, performance of CCPSO-m is much better than the other algorithms in this large-scale MPPT application.

In a word, MPP of each photovoltaic module (or MCU) can be tracked effectively. The new photovoltaic system can avoid “hot spot” problem and achieve maximum output power under complex environmental conditions. In future, more efforts will be made to simplify the large-scale optimization algorithm and to improve the accuracy of mathematical model of photovoltaic module. New methods that can reduce time cost of the MPPT process are also parts of future work.

Acknowledgment

This work was supported by the National Natural Science Foundation of China under Grants 61201168 and 51377187.

References

- Abdelsalam, A.K., Massoud, A.M., Ahmed, S., Enjeti, P., 2011. High-performance adaptive perturb and observe MPPT technique for photovoltaic-based microgrids. *IEEE Trans. Power Electron* 26 (4), 1010–1021.
- Atmaca, E., 2015. Energy management of solar car in circuit race. *Turkish J. Electr. Eng. Comput. Sci.* 23 (4), 1142–1158.
- Benyoucef, A.S., Chouder, A., Kara, K., Silyestre, S., Sahed, O.A., 2015. Artificial bee colony based algorithm for maximum power point tracking (MPPT) for PV systems operating under partial shaded conditions. *Appl. Soft Comput.* 32, 38–48.
- Chen, W.Y. et al., 2013. Research on MPPT of PV system based on SVM model. *Acta Energetica Solaris Sin.* 34 (2), 245–250.
- Choi, W.Y., Lai, J.S., 2010. High-efficiency grid-connected photovoltaic module integrated converter system with high-speed communication interfaces for small-scale distribution power generation. *Sol. Energy* 84 (4), 636–649.
- Clerc, M., Kennedy, J., 2002. The particle swarm-explosion, stability, and convergence in a multidimensional complex space. *IEEE Trans. Evol. Comput.* 6 (1), 58–73.
- d’Alessandro, V., Guerriero, P., Daliento, S., 2014. A simple bipolar transistor-based bypass approach for photovoltaic modules. *IEEE J. Photovoltaics* 4 (1), 405–413.
- Dein, M.Z.S.E.I., Kazerani, M., Salama, M.M.A., 2013. Optimal photovoltaic array reconfiguration to reduce partial shading losses. *IEEE Trans. Sustain. Energy* 4 (4), 145–153.
- Eberhart, R.C., Shi, Y., 2000. Comparing inertia weights and constriction factors in particle swarm optimization. In: *Proceedings of the IEEE Congress on Evolutionary Computation*, pp. 84–89.
- Femia, N., Petrone, G., Spagnuolo, G., Vitelli, M., 2005. Optimization of perturb and observe maximum power point tracking method. *IEEE Trans. Power Electron* 20 (4), 963–973.
- Girish, T.E., Aranya, S., Nisha, N.G., 2007. Photovoltaic power generation using albedo and thermal radiations in the satellite orbits around planetary bodies. *Sol. Energy Mater. Sol. Cells* 91 (15–16), 1503–1504.
- Jubaer, A., Zainal, S., 2015. An improved perturb and observe (P&O) maximum power point tracking (MPPT) algorithm for higher efficiency. *Appl. Energy* 150, 97–108.
- Kaabeche, A., Ibtouen, R., 2014. Techno-economic optimization of hybrid photovoltaic/wind/diesel/battery generation in a standalone power system. *Sol. Energy* 103 (6), 171–182.
- Kibria, M.A., Saidur, R., Al-Sulaiman, F.A., Aziz, M.M.A., 2016. Development of a thermal model for a hybrid photovoltaic module and phase change materials storage integrated in buildings. *Sol. Energy* 124, 114–123.
- Koutroulis, E., Kalaitzakis, K., Voulgaris, N.C., 2001. Development of a microcontroller-based photovoltaic maximum power point tracking control system. *IEEE Trans. Power Electron* 16 (1), 46–54.
- Kulaksiz, A.A., Akkaya, R., 2012. A genetic algorithm optimized ANN-based MPPT algorithm for a stand-alone PV system with induction motor drive. *Sol. Energy* 86 (9), 2366–2375.
- Lai, J.G., et al., 2016. Droop-based distributed cooperative control for microgrids with time-varying delays. *IEEE Trans. Smart Grid*, <http://dx.doi.org/10.1109/TSG.2016.2557813>.

- Laudani, A., Fulginei, F.R., Salvini, A., 2014. Identification of the one-diode model for photovoltaic modules from datasheet values. *Sol. Energy* 108, 432–446.
- Lee, D.Y., Cutler, J.W., Mancewicz, J., Ridley, A.J., 2015. Maximizing photovoltaic power generation of a space-dart configured satellite. *Acta Astronaut.* 111, 283–299.
- Lei, L., 2011. Study on Maximum Power Point Tracking of Partially Shaded Photovoltaic System. Chongqing University, Chongqing, China.
- Liu, Y.L., Zhou, H., Cheng, Z., 2010. MPPT control method of PV system based on PSO. *Comput. Eng.* 36 (15), 265–267.
- Li, X.D., Yao, X., 2009. Tackling high dimensional nonseparable optimization problems by cooperatively coevolving particle swarms. In: *Proceedings of the IEEE Congress on Evolutionary Computation*, pp. 1546–1553.
- Li, X.D., Yao, X., 2012. Cooperatively coevolving particle swarms for large scale optimization. *IEEE Trans. Evol. Comput.* 16 (2), 210–224.
- Maki, A., Valkealahti, S., 2013. Effect of photovoltaic generator components on the number of MPPs under partial shading conditions. *IEEE Trans. Energy Convers.* 28 (4), 1008–1017.
- Moreton, R., Lorenzo, E., Narvarte, L., 2015. Experimental observations on hot-spots and derived acceptance/rejection criteria. *Sol. Energy* 118, 28–40.
- Nafeh, A.E.S.A., 2011. A modified MPPT control loop for PV/battery-charging system using PI controller optimally tuned with GA. In: *J. Numer. Modell. – Electron. Networks Dev. Fields* 24 (2), 111–122.
- Pennisi, S., Pulvirenti, F., Scala, A.L., 2011. Low-power cool bypass switch for hot spot prevention in photovoltaic panels. *ETRI J.* 33 (6), 880–886.
- Petrone, G., Spagnuolo, G., Vitelli, M.A., 2011. Multivariable perturb-and-observe maximum power point tracking technique applied to a single-stage photovoltaic inverter. *IEEE Trans. Industr. Electron.* 58 (1), 76–84.
- Piegari, L., Rizzo, R., 2010. Adaptive perturb and observe algorithm for photovoltaic maximum power point tracking. *Renew Power Generation IET* 4 (4), 317–328.
- Pierro, M., Bucci, F., Cornaro, C., 2015. Full characterization of photovoltaic modules in real operating conditions: theoretical model, measurement method and results. *Progr. Photovoltaics* 23 (4), 443–461.
- Potter, M., Jong, K.D., 1994. A cooperative coevolutionary approach to function optimization. In: *Proceedings of the 3rd Conference on Parallel Problem Solving*, pp. 249–257.
- Qin, A.K., Suganthan, P.N., 2005. Self-adaptive differential evolution algorithm for numerical optimization. In: *Proceedings of the IEEE Congress on Evolutionary Computation*, pp. 1785–1791.
- Radjai, T., Rahmani, L., Mekhilef, S., Gaubert, J.P., 2014. Implementation of a modified incremental conductance MPPT algorithm with direct control based on a fuzzy duty cycle change estimator using dSPACE. *Sol. Energy* 110, 325–337.
- Renaudineau, H. et al., 2015. APSSO-based global MPPT technique for distributed PV power generation. *IEEE Trans. Industr. Electron.* 62 (2), 1047–1058.
- Shaiek, Y., Smida, M.B., Sakly, A., Mimouni, M.F., 2013. Comparison between conventional methods and GA approach for maximum power point tracking of shaded solar for PV generators. *Sol. Energy* 90 (4), 107–122.
- Shi, J.Y., Zhang, W., 2014. MPPT for PV systems based on a dormant PSO algorithm. *Electric Power Syst. Res.* 123, 100–107.
- Su, J.H. et al., 2001. Investigation on engineering analytical model of silicon solar cells. *Acta Energetica Solaris Sin.* 22 (4), 409–412.
- Sullivan, C.R., Awerbuch, J.J., Latham, A.M., 2013. Decrease in photovoltaic power output from ripple: simple general calculation and the effect of partial shading. *IEEE Trans. Power Electron.* 28 (2), 740–747.
- Tey, K.S., Mekhilef, S., 2014. Modified incremental conductance algorithm for photovoltaic system under partial shading conditions and load variation. *IEEE Trans. Industr. Electron.* 61 (10), 5384–5392.
- Van den Bergh, F., Engelbrecht, A., 2004. A cooperative approach to particle swarm optimization. *IEEE Trans. Evol. Comput.* 8 (3), 225–239.
- Vinnichenko, N.A., Uvarov, A.V., Znamenskaya, I.A., Ay, H., Wang, T.H., 2014. Solar car aerodynamic design for optimal cooling and high efficiency. *Sol. Energy* 103 (6), 183–190.
- Wu, Z., Xia, X., 2015. Optimal switching renewable energy system for demand side management. *Sol. Energy* 114, 278–288.
- Xu, F., Zhang, R., Wu, L.B., Xu, H.W., 2012. Self-adaption BP neural network for the maximum-power-point tracking in photovoltaic. *Acta Energetica Solaris Sin.* 33 (3), 468–472.
- Yang, Z.Y., Tang, K., Yao, X., 2008. Large scale evolutionary optimization using cooperative coevolution. *Information Sci.* 178 (15), 2985–2999.
- Yin, C., Chen, Y.Q., Zhong, S.M., 2014. Fractional-order sliding mode based on extremum seeking control of a class of nonlinear systems. *Automatica* 50 (12), 3173–3181.
- Yin, C. et al., 2015. Fractional-order adaptive minimum energy cognitive lighting control strategy for the hybrid lighting system. *Energy Build.* 87 (7), 176–184.
- Zan, B.L., Song, Y.D., Wang, L., Wang, Y.H., Du, X.Q., Zeng, Y., 2013. An improved P&O MPPT method for photovoltaic power system. *Energy and power technology PTS 1 and 2*, 805–806, pp. 45–51.
- Ziar, H., Nouri, M., Asaei, B., Farhangi, S., 2014. Analysis of overcurrent occurrence in photovoltaic modules with overlapped by-pass diodes at partial shading. *IEEE J. Photovoltaics* 4 (2), 713–721.